Breathing mode of a skyrmion on a lattice

Dmitry A. Garanin,[1] Reem Jaafar,[2] and Eugene M. Chudnovsky[1]
[1]*Physics Department, Herbert H. Lehman College and Graduate School, The City University of New York, 250 Bedford Park Boulevard West, Bronx, New York 10468-1589, USA*
[2]*Department of Mathematics, Engineering and Computer Science, LaGuardia Community College, The City University of New York, 31-10 Thomson Avenue, Long Island City, New York 11101, USA*

(Received 4 June 2019; revised manuscript received 28 July 2019; published 14 January 2020)

The breathing modes of a skyrmion, corresponding to coupled oscillations of its size and chirality angle, are studied numerically for a conservative classical-spin system on a 500 × 500 lattice. The dependence of the oscillation frequency on the magnetic field is computed for a model with Dzyaloshinskii-Moriya interaction. In accordance with previous works, it is linear at small fields, reaches maximum on increasing the field, then sharply tends to zero as the field approaches the threshold above which the skyrmion loses stability and collapses. Physically transparent analytical model is developed that explains the results qualitatively and provides the field dependence of the oscillation frequency that is close to the one computed numerically. Dissipation of a breathing motion in which the skyrmion chirality angle γ is rotating in one direction depends on the initial amplitude. Below a certain threshold the mode is stable, while above that threshold it becomes strongly damped by the reservoir of spin waves and quickly ends with the skyrmion collapse. To the contrary, smaller-amplitude breathing motion in which γ oscillates is undamped in the absence of other interactions. Adding perpendicular anisotropy and removing the applied field makes the breathing mode of any amplitude very slow and undamped.

DOI: 10.1103/PhysRevB.101.014418

I. INTRODUCTION

Studies of skyrmions have opened a promising avenue for developing new forms of memory storage and information processing [1–7]. Skyrmions in thin films are defects of the uniformly magnetized ferromagnetic state stabilized by topology. They had been first introduced in the nonlinear σ model by Skyrme [8] and later intensively studied in nuclear physics [9]. Their topological properties in a two-dimensional (2D) Heisenberg exchange model have been elucidated by Belavin and Polyakov (BP) [10,11]. In practice, topological stability of skyrmions that arises from the continuous field model is violated in solids by the discreteness of the atomic lattice [12]. External magnetic field, magnetic anisotropy, dipole-dipole interaction (DDI), thermal and quantum fluctuations, etc., further break the symmetry of the exchange model, leading to the uncontrolled collapse or expansion of skyrmions. For that reason, they are typically observed in noncentrosymmetric materials. In such materials, the Dzyaloshinskii-Moriya interaction (DMI) that arises from the lack of the inversion symmetry provides stability of skyrmions within a certain area of the phase diagram [5,13]. To date, stable isolated skyrmions have been experimentally observed at room temperatures [7,14,15]. It has been demonstrated that the size of a skyrmion can be tuned by the external magnetic field, with its radius shrinking on increasing the field opposite to the skyrmion's spin until the skyrmion disappears [16,17].

The shape of the smallest skyrmions is typically close to the shape (see Fig. 1) provided by the BP solution of the pure exchange model [18], while bigger skyrmions resemble magnetic bubbles studied in the past [19]. Field-theoretical approach to the internal dynamics of skyrmions in nuclear physics and 2D magnets goes back to the 1980's [20,21]. More recently, the interest to the internal modes of skyrmions stabilized by the DMI has developed [22].

Chiral spin-wave modes of skyrmions and edge oscillations of skyrmion bubbles, including a breathing-type mode, have been predicted [23,24] and experimentally observed [25] in skyrmion crystals. A translational mode and different type of breathing modes have been calculated for isolated skyrmions using Landau-Lifshitz-Gilbert (LLG) dynamics in Ref. [26]. Linear dependence of the frequency of the breathing mode on the field has been found [26,27] with the slope close to 80% of the slope of the ferromagnetic resonance frequency. Both papers are solving the eigenvalue problem after linearizing equations of motion around the numerically found skyrmion state. Their result will be confirmed by our calculations that use a different numerical method.

Breathing mode near skyrmion collapse on approaching the critical field H_c has been addressed by Rózsa *et al.* [28] who showed that the frequency of the mode rapidly approaches zero at $H \to H_c$. This will also be confirmed by our method. Hybridization of breathing modes with quantized spin-wave modes in circular ultrathin magnetic dots have been studied via micromagnetic computations [29]. The role of the internal modes in the problem of the skyrmion mass has been investigated [30,31].

Most recently, the breathing dynamics of skyrmions and antiskyrmions that are large compared to the domain-wall width has been analyzed by McKeever *et al.* [32]. Their analytical method modifies the Lagrangian formalism for the skyrmion size and chirality angle used in Refs. [18,31] by including damping due to other degrees of freedom (such as phonons, nuclear spins, itinerant electrons, defects,

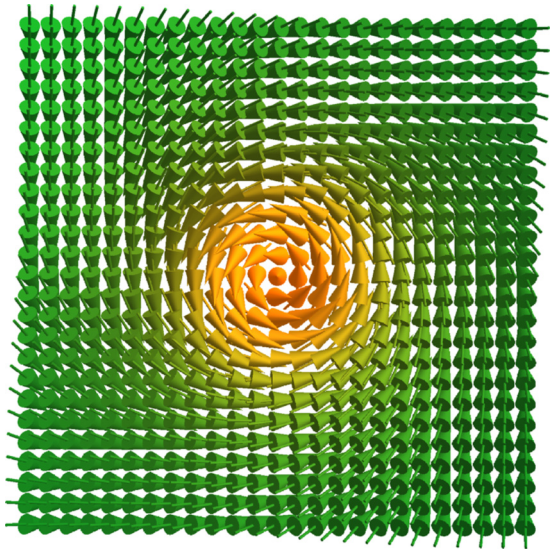

FIG. 1. Spin field in a Bloch-type skyrmion studied in the paper. Its breathing mode corresponds to the coupled oscillations of the skyrmion size and spin angles.

electromagnetic radiation, etc.) via the Rayleigh dissipative functional. Reference [32] makes an interesting observation of the two different breathing modes, oscillatory and rotational, with the first decaying exponentially and the second decaying linearly with time.

The breathing mode of a skyrmion shown in Fig. 1 corresponds to coupled oscillations of its size and its spin angles. In this paper, we first confirm previously obtained results [26–28], including the 0.8 slope, through numerical computation of the spin dynamics on 2D lattices of size ranging from 100×100 to 500×500. We checked that results are independent of the system size in the limit of the large lattice. At small amplitude, the oscillation frequency is linear on the field at weak fields, reaches maximum in the critical region, and tends to zero as the field approaches the collapse threshold. The fact that the frequency of that internal skyrmion mode is below the spin-wave spectrum of the uniformly magnetized ferromagnetic state explains why no dissipation of the breathing mode has been observed in the numerical experiment when no damping has been introduced by hand.

We then study the breathing mode within analytical and semianalytical models based upon Lagrangian dynamics of the skyrmion [18]. While our analytical results agree with numerical results within 20%, they provide a transparent physical picture of the field dependence of the breathing mode in the entire field range.

We then move to the study of the large-amplitude oscillations by solving the conservative model of classical spins on a lattice. We find that the dynamics of the breathing motion in which the skyrmion chirality angle rotates in one direction instead of oscillating depends strongly on the initial amplitude. For a sufficiently small amplitude the mode is stable, although its dynamics is affected by the bulk spin-wave modes. Above a certain threshold, the large-amplitude mode becomes strongly damped by the emission of spin waves. Such oscillations end quickly with the skyrmion collapse. This result complements the findings of Ref. [32]. One-to-one correspondence between the two works is not expected since we do not consider the limit of a skyrmion large compared to the domain-wall width and do not introduce phenomenological damping.

The paper is structured as follows. The model, the numerical method, and the results for the small-amplitude skyrmion breathing mode computed on a lattice are given in Sec. II. Section III contains one crude qualitative approach and another more refined semianalytical approach to skyrmion internal oscillations that provide clear physical interpretation of the numerical results. Dynamics of large-amplitude breathing modes is considered in Sec. IV. Our conclusions are summarized in Sec. V.

II. SKYRMION BREATHING MODE IN THE LATTICE MODEL

A. General

We consider a two-dimensional square lattice of normalized classical spins $\mathbf{s}_i \equiv \mathbf{S}_i/S$, where $\mathbf{S}_i$ is a three-dimensional vector and $i = \{i_x, i_y\}$ refers to the lattice site. The Hamiltonian of the system is given by

$$\mathcal{H} = -\frac{S^2}{2}\sum_{ij} J_{ij}\mathbf{s}_i \cdot \mathbf{s}_j - HS\sum_i s_{iz} - \frac{DS^2}{2}\sum_i s_{iz}^2 - AS^2 \sum_{i_x,i_y} \left(\mathbf{s}_{i_x-1,i_y} \times \mathbf{e}_x + \mathbf{s}_{i_x,i_y-1} \times \mathbf{e}_y\right) \cdot \mathbf{s}_{i_x,i_y}. \quad (1)$$

The first term represents the Heisenberg exchange energy with the exchange constant J and the sum is taken over the nearest neighbors. The second term is the Zeeman interaction energy due to the external field H normal to the xy plane. The third term is the energy of the perpendicular magnetic anisotropy (PMA) of strength D. The last term represents the Dzyaloshinskii-Moriya interaction (DMI) of strength A. For certainty, we have chosen the Bloch-type DMI that favors the Bloch-type skyrmions shown in Fig. 1 (spins rotating counterclockwise for $A > 0$).

The presence of the skyrmion in the system is revealed by a nonzero topological charge:

$$Q = \frac{1}{4\pi}\int dx\, dy\, \mathbf{s} \cdot \left(\frac{\partial \mathbf{s}}{\partial x} \times \frac{\partial \mathbf{s}}{\partial y}\right) \quad (2)$$

that takes discrete values $Q = 0, \pm 1, \pm 2, \ldots$. In numerical work we compute the discretized version of this expression.

Within the purely exchange continuous model, the BP solution for the skyrmion with $Q = 1$ and spins in the center of the skyrmion pointing up against the spin-down background in terms of polar coordinates $x = r\cos\phi$, $y = r\sin\phi$ has the form

$$\begin{Bmatrix} s_x \\ s_y \end{Bmatrix} = \frac{2\lambda r}{r^2+\lambda^2}\begin{Bmatrix} \cos(\phi+\gamma) \\ \sin(\phi+\gamma) \end{Bmatrix}, \quad s_z = \frac{\lambda^2 - r^2}{\lambda^2 + r^2}. \quad (3)$$

Here, λ is the skyrmion size and spins are rotated away from the radial direction by the chirality angle γ. The energy of the skyrmion is independent of λ and γ and equal to $4\pi JS^2$ above that of the uniform state. This is the invariance found by Belavin and Polyakov.

It was shown that the discreteness of the lattice makes the energy decrease with decreasing λ that leads to the skyrmion collapse [12]. Other interactions apart from the exchange also break the invariance. The PMA leads to the energy increase with λ, thus, it should lead to a collapse. However, the dipole-dipole interaction favors the skyrmion expansion and, together with the PMA, it can stabilize the skyrmion at a particular size. DMI favors skyrmion expansion and adjustment of the chirality angle to a particular value ($\gamma = \pi/2$ for the Bloch DMI with $A > 0$). This expansion can be limited by the magnetic field applied in the negative direction with respect to the skyrmion's spin. This stabilizes the skyrmion at a particular size. If the applied field becomes too strong, the skyrmion collapses.

Certainly, the shape of the skyrmion stabilized by nonexchange interactions differs from the BP shape. However, since the exchange is the strongest interaction, at least small skyrmions are only weakly distorted. Thus, if makes sense to use Eq. (3) as the ansatz in the analytical approach. Below, we will ignore the DDI and mainly investigate the model with the DMI, numerically and analytically, focusing on the breathing mode.

The breathing mode is the lowest-frequency local mode of the skyrmion in which the skyrmion size is oscillating around its equilibrium value. As we will see, this is accompanied by oscillations of the dynamically conjugate variable, the chirality angle γ. There should be faster modes including various deformations of the skyrmion, that will not be investigated.

B. Numerical energy minimization and the skyrmion size

To find the frequency of the breathing mode numerically, first the energy minimization was done for a particular set of parameters. The main choice was $A/J = 0.02$, whereas the applied field H changed between its collapse value and zero. As the initial condition, any bubble with $Q = 1$ at the center of the system can be used. The numerical method [33] combines sequential rotations of spins $\mathbf{s}_i$ toward the direction of the local effective field

$$\mathbf{H}_{\text{eff},i} = -\partial\mathcal{H}/\partial\mathbf{s}_i, \tag{4}$$

with the probability α, and the energy-conserving spin flips (over-relaxation)

$$\mathbf{s}_i \to 2(\mathbf{s}_i \cdot \mathbf{H}_{\text{eff},i})\mathbf{H}_{\text{eff},i}/H^2_{\text{eff},i} - \mathbf{s}_i, \tag{5}$$

with the probability $1 - \alpha$. We used $\alpha = 0.03$ that ensures the fastest relaxation. This procedure leads to the same results as solution of coupled Landau-Lifshitz equations for the spins. It was found that the breathing mode can be seen only in the model with periodic boundary conditions (pbc), both for the exchange and for the DMI. In the case of free boundary conditions, there are surface modes that interfere in the extraction of the frequency of the breathing mode. Thus, all computation were performed on the model with pbc.

The skyrmion size λ can be extracted from the numerical data as [12]

$$\lambda_n^2 = \frac{n-1}{2^n\pi}a^2\sum_i (s_{iz}+1)^n, \tag{6}$$

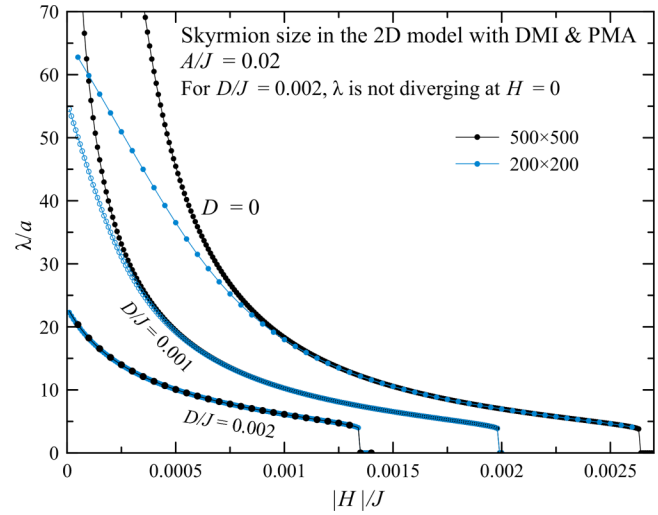

FIG. 2. Skyrmion size vs the applied magnetic field computed on 200×200 and 500×500 lattices for $A/J = 0.02$ and PMA values $D = 0$ and $0.001J$.

where a is the lattice spacing. In our case $s_{iz} = -1$ in the background and $s_{iz} = 1$ at the center of the skyrmion. For the BP skyrmions with s_z given by Eq. (3), one has $\lambda_n = \lambda$ for any n. In this paper, we used $\lambda = \lambda_4$ to represent the numerically computed skyrmion size. We also computed the components of the average spin of the system as

$$\mathbf{m} = \frac{1}{N}\sum_i \mathbf{s}_i. \tag{7}$$

One can also define the skyrmion spin as

$$\mathcal{M} = \sum_i (s_{iz}+1). \tag{8}$$

The angle γ was extracted by building the sum of dot products of the lattice spins $\mathbf{s}_i$ by the radial vectors $\mathbf{r}_i$ (with respect to the center of the lattice), that yields $\cos\gamma$, and by the $\boldsymbol{\phi}_i$ vectors, that are perpendicular to the $\mathbf{r}_i$ vectors and point counterclockwise, to find $\sin\gamma$.

The results for the equilibrium skyrmion size vs H for two different system sizes, $A/J = 0.02$, and three different values of the PMA, $D/J = 0$, 0.001, and 0.002, are shown in Fig. 2. For $D = 0$, the skyrmion size diverges in the limit $H \to 0$. However, the divergence is limited by the system size that is clearly seen in the figure. Thus, for a small field, a large system size is needed. PMA tends to decrease the skyrmion size, thus for $D/J = 0.001$ the latter is noticeably smaller, while the collapse field is smaller, too. The skyrmion size still diverges for $H \to 0$. To the contrary, for a stronger PMA, $D/J = 0.002$, the skyrmion size does not diverge and the results for both system sizes are the same. This means that a sufficiently strong PMA can stabilize the skyrmion at $H = 0$. On the other hand, if the PMA becomes too strong, the skyrmion will collapse. Thus, there is a range of D that stabilize the skyrmion at $H = 0$.

C. Numerical dynamics of the breathing mode

After the equilibrium skyrmion configuration was found, the frequency of its oscillations around the equilibrium was measured by running the dynamical evolution following the initial global rotation of all spins in the system by a small angle $\Delta\gamma$ around the z axis. We used the fourth-order Runge-Kutta ordinary-differential-equation solver with the integration step 0.2 in the units of $\hbar/J$ to solve the system of Larmor equations of motion

$$\dot{\mathbf{s}}_i = \frac{1}{\hbar}\mathbf{s}_i \times \mathbf{H}_{\mathrm{eff},i} \tag{9}$$

with $\mathbf{H}_{\mathrm{eff},i}$ given by Eq. (4) for the lattice spins (in the computations we set $\hbar \Rightarrow 1$). No damping was included in this computation because in many-spin systems there can be intrinsic damping, e.g., via the conversion of the energy of the initial state into that of spin waves via different kinds of linear and nonlinear processes (see Ref. [34] and references therein). Including the phenomenological damping via the Landau-Lifshitz equation will obscure the intrinsic processes.

For the small DMI constant and the applied field used here, the dynamics is rather slow, so that the discretization error of the Runge-Kutta method is rather small. The length of spin vectors and the energy of the system practically do not change over large time intervals. However, one cannot significantly increase the step as already for the step 0.3 an instability occurs due to the exchange term in the equations.

The computation was done independently for each value of H in parallel using Worfram *Mathematica* with vectorization and compilation on a 20-core Dell Precision Workstation (16 cores used by *Mathematica*). Computations performed for $A/J = 0.1, 0.02, 0.01$ show qualitatively similar behavior. In the paper, most of the results are given for $A/J = 0.02$ with $D/J = 0$ and $D/J = 0.002$. They were computed for the system sizes 100×100, 200×200, 300×300, 400×400, and 500×500. A greater system size is needed for small applied fields when the skyrmion size becomes large. Comparison of the results for different system sizes show that at our maximal size 500×500 there are no finite-size effects in the main range of H, except for the smallest H.

It was found that the skyrmion size λ and the system's average spin m_z (or, equivalently, the skyrmion's magnetic moment $\mathcal{M}$) performed periodic oscillations with a weak anharmonicity (see Fig. 3). Since the curves for m_z are smoother than those for λ, the former were used to extract the oscillation frequency. The time interval between the adjacent maximum and minimum (or between a minimum and a maximum) of m_z was interpreted as the half of the period to extract the oscillation frequency. This half-period of the evolution costs much more computer time than finding the skyrmion's equilibrium state in the first stage. In the parallelized computation for different values of H, after reaching the first maximum and the first minimum of m_z, the computation was terminated and the frequency was recorded.

The anharmonicity of $\lambda(t)$ could be attributed to a weak hybridization of the breathing mode with the other local modes (see, e.g., Ref. [35]) that also could be excited by rotating all spins by $\Delta\gamma$. Indeed, the deviation from the equilibrium skyrmion state can be expanded over the set of local modes. In this expansion, the breathing mode should be the strongest

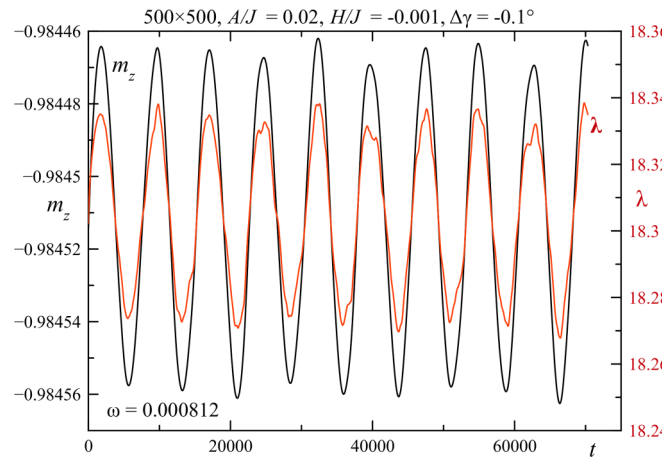

FIG. 3. Numerically obtained oscillations of m_z and of the skyrmion size λ in the breathing mode computed on a 500×500 lattice for $A/J = 0.02$, $H/J = -0.001$, and $\Delta\gamma = -0.1^\circ$. Time is measured in units of $\hbar/J$.

while other modes enter with smaller weights and thus they distort the breathing dynamics to some extent seen in the dependencies $\lambda(t)$ and $m_z(t)$.

On the other hand, no damping of the breathing mode was detected. One can argue that its frequency always falls below the frequency of the uniform precession, thus the breathing mode is not resonating with the spin-wave band. However, in Sec. IV we will see that large-amplitude breathing mode can relax via nonresonant processes as well. Here, it is important that the amplitude of the breathing mode is small and the spin rotation periodically changes its direction while in spin waves spin precession is unidirectional. This impedes the energy transfer between these modes.

The dependence of the frequency of the breathing mode on the magnetic field at $D = 0$ is shown in Fig. 4. The $\omega(H)$ curves obtained numerically on lattices of different size have little size dependence, except for weak fields, where $\omega(H)$ has a size-dependent uptick. Here, one can expect skyrmions branching out and transform to a laminar domain state. The $\omega(H)$ curves exhibit a characteristic maximum on approach to the critical field above which the skyrmion collapses. Here, $\omega(H)$ goes to zero steeply. On the left side of the maximum, where skyrmions are big and the lattice discreteness becomes unimportant, $\omega(H)$ goes apparently linearly and can be approximated by the dependence $\hbar\omega(H) = 0.8H$ in accordance with findings of other authors [26,27]. Similarly, the drop of $\omega(H)$ toward zero at $H \to H_c$ agrees with the result of Ref. [28]. Qualitatively similar behavior is exhibited by the $\omega(H)$ curves computed analytically in the next section, that are shown in the same figure.

It is remarkable that the dependence $\hbar\omega(H) = 0.8H$ holds for different values of the DMI constant A. Thus, the slope 0.8 that appears in Figs. 4–6 is a universal number. Note that in the limit of $H \to 0$ the skyrmion becomes very large. In that limit, our model may not be catching the spin field in the skyrmion correctly and this must be the reason for the observed deviation from the linear behavior.

Numerical results in the presence of the PMA are shown in Fig. 6 for $A/J = 0.02$ and the system size 500×500. In

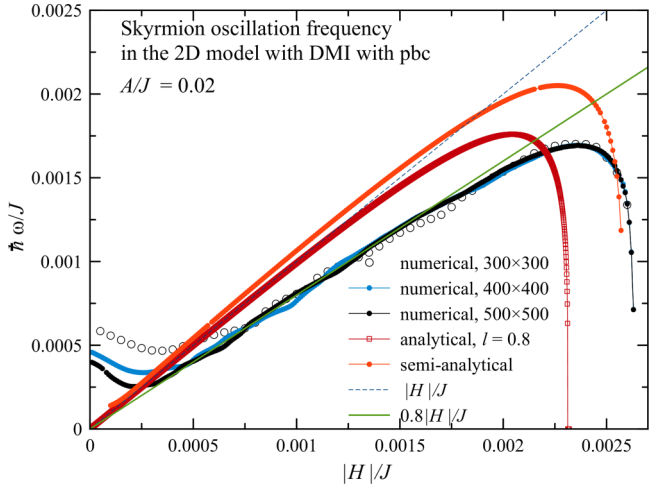

FIG. 4. Field dependence of the oscillation frequency of the breathing mode computed numerically on lattices of different sizes, analytically for a BP skyrmion shape with logarithmic accuracy, and semianalytically in a model with the skyrmion shape corrected (see Sec. III for the definition of parameter l). The slope of the straight-line part of the spectrum computed analytically in models that ignore spin waves roughly coincides with the ferromagnetic resonance (FMR) slope. The slope computed by the numerical method that accounts for all excitations in the system is close to 0.8 of the FMR slope, which agrees with Refs. [26,27].

accordance with Fig. 2, the collapse fields and the entire curves shift to the left with increasing the PMA. The breathing-mode frequency $\omega(H)$ is well below the ferromagnetic resonance (FMR) frequency

$$\omega_{\mathrm{FMR}} = (D + H)/\hbar. \tag{10}$$

For $D/J = 0.001$, $\omega(H)$ goes to zero with a high slope at $H \to 0$. This must be related to the divergence of $\lambda(H)$ seen in Fig. 2. To the contrary, for $D/J = 0.002$, the breathing-mode frequency remains finite at $H = 0$ that correlates with the finite λ at zero field in Fig. 2.

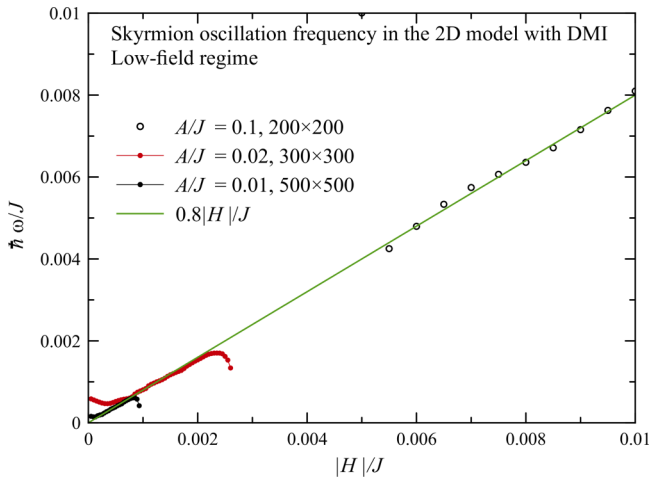

FIG. 5. Frequency of the breathing mode in the linear-H regime computed on lattices of different size for different values of the DMI constant A.

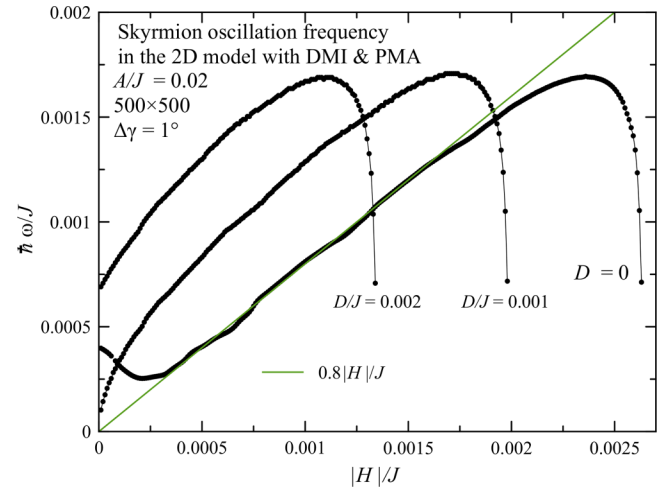

FIG. 6. Breathing-mode frequency vs the applied magnetic field for $A/J = 0.02$ and different PMA values.

It is nontrivial that at $D = 0$ the frequency of the breathing mode in the main region of the applied field follows, for any value of A, a linear law $\hbar\omega(H) = 0.8H$ that is resembling that for the FMR frequency $\hbar\omega_{\mathrm{FMR}} = H$ but has a smaller coefficient. In fact, the breathing mode and the bulk-precession mode have totally different structures. In the precession mode, $m_z = \mathrm{const}$ while m_x and m_y are precessing. In the breathing mode, m_z is oscillating, while the spin orientation quantified by the angle γ is performing small oscillations around its equilibrium value. These two main modes are independent at small amplitudes and can coexist. To check this, we initiated dynamics by rotating all spins by 0.1° around the y and then around the z axes. This excites both modes, the temporal evolution of which is shown in Fig. 7. One can see that the frequencies of these modes are different. Moreover, rotation of spins only around the z axis, to excite the breathing mode, also excites the bulk precession mode with a very small, although

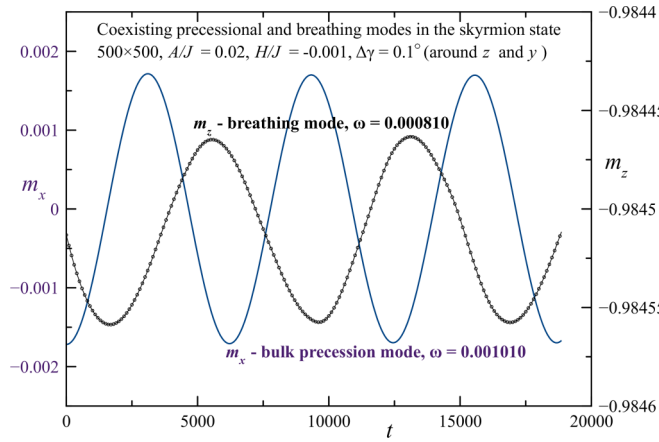

FIG. 7. Coexisting breathing and bulk precession modes after rotating spins around z and and then around y axes out of the equilibrium-skyrmion state, computed for $A/J = 0.02$, $H/J = -0.001$, and $\Delta\gamma = 0.1^\circ$. These modes oscillate at close but distinctly different frequencies.

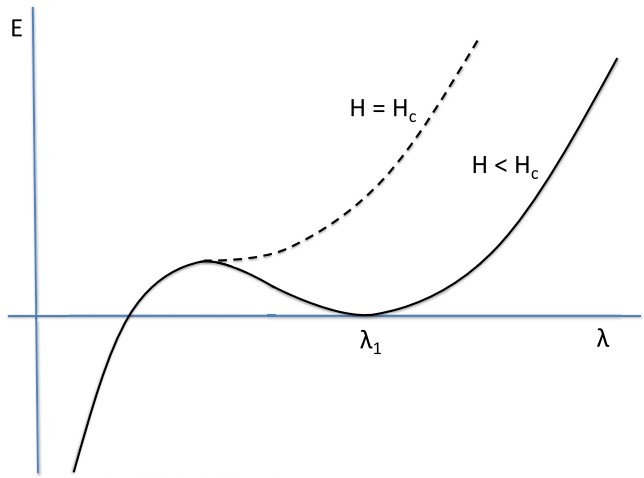

FIG. 8. Qualitative dependence of the skyrmion energy on skyrmion size λ for $\gamma = \pi/2$. The minimum corresponding to the equilibrium size disappears for $H > H_c$. At $H = H_c$ the energy has an inflection point where both first and second derivatives are zero.

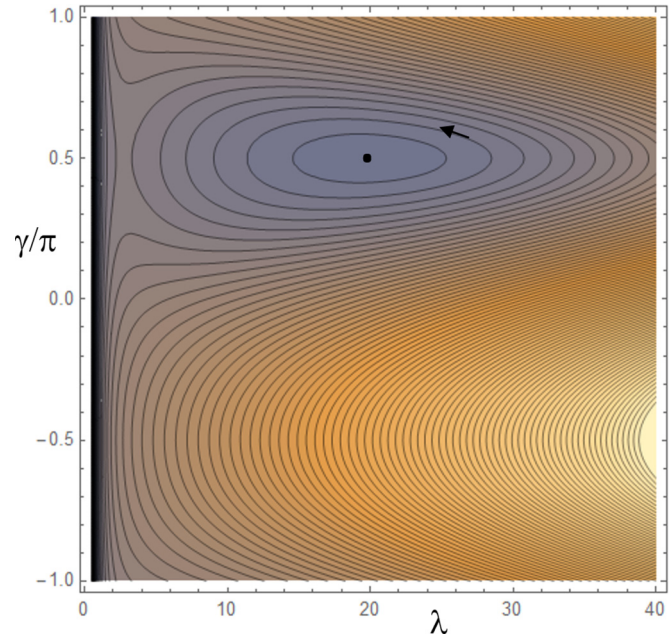

FIG. 9. Equipotential lines in the $\{\lambda, \gamma\}$ plane corresponding to Eq. (12) with $l = \text{const}$.

numerically detectable amplitude, evolving with the proper FMR frequency.

III. SKYRMION BREATHING MODE IN A SPIN-FIELD MODEL

A. Analytical approach with the BP ansatz for the skyrmion shape

The fact that $\omega(H)$ tends to zero at the critical field $H = H_c$ can be easily understood from the dependence of the energy on the field and the size of the skyrmion shown in Fig. 8. Skyrmion of a stable size exists at $H > H_c$ when $E(\lambda)$ has a minimum. At $H = H_c$ the minimum becomes an inflection point where both first and second derivatives of E on λ are zero. It is the nullification of the second derivative that makes the frequency of the breathing mode zero at $H = H_c$. In this section we develop analytical approach that elucidates the dynamics of the breathing mode in simple physical terms.

The continuous analog of Eq. (1) is

$$\mathcal{H} = \frac{JS^2}{2}\int dx\,dy\left[\left(\frac{\partial \mathbf{s}}{\partial x}\right)^2 + \left(\frac{\partial \mathbf{s}}{\partial y}\right)^2\right] - \frac{JS^2a^2}{24}\int dx\,dy\left[\left(\frac{\partial^2 \mathbf{s}}{\partial x^2}\right)^2 + \left(\frac{\partial^2 \mathbf{s}}{\partial y^2}\right)^2\right] - \frac{HS}{a^2}\int dx\,dy\,s_z - \frac{DS^2}{2a^2}\int dx\,dy\,s_z^2 + \frac{AS^2}{a}\int dx\,dy\left(\frac{\partial \mathbf{s}}{\partial x}\times \mathbf{e}_x + \frac{\partial \mathbf{s}}{\partial y}\times \mathbf{e}_y\right)\cdot \mathbf{s}. \quad (11)$$

The second term in this expression arises from taking into consideration the next derivatives in the expansion of the discrete form of the exchange energy that dominates spin interactions at small distances. The spin combination in the DMI energy can be rewritten as $\mathbf{s}\cdot(\nabla\times\mathbf{s})$. For a small skyrmion that is close to the BP shape, substitution of Eq. (3) into Eq. (11) gives at $D = 0$ [18]

$$\bar{E} \equiv \frac{\mathcal{H}}{4\pi JS^2} = h\bar{\lambda}^2 l(\bar{\lambda}) - \frac{1}{6\bar{\lambda}^2} - \alpha\bar{\lambda}\,\sin\gamma, \quad (12)$$

where $h \equiv H/(JS)$, $\alpha \equiv A/J$, $\bar{\lambda} \equiv \lambda/a$, and $l(\bar{\lambda})$ has a logarithmic dependence on λ that is sensitive to the shape of the skyrmion far from its center. This function for $\gamma = \pi/2$ is shown qualitatively in Fig. 8. The energy minimum corresponding to a stable skyrmion disappears at $H > H_c$ where H_c is the critical field computed below. The existence of such a field is known from experiments. Above it, the skyrmion collapses irreversibly. This effect is due to the second term in Eq. (12) that originates from the discreetness of the atomic lattice [12].

Consider first a crude approximation with $l = \text{const}$. The whole potential landscape of Eq. (12) is shown in Fig. 9 for $\alpha = 0.02$, $h = -0.001$, and $l = 0.5$. As the dynamics of the skyrmion conserves the energy, the system is moving in its phase space $\{\lambda, \gamma\}$ along the equipotential lines. The motion occurs in the counterclockwise direction. The center point is the energy minimum $\gamma = \pi/2$ and $\lambda = \lambda_1$ defined by the algebraic equation

$$\frac{\partial \bar{E}}{\partial \bar{\lambda}} = 2lh\bar{\lambda} + \frac{1}{3\bar{\lambda}^3} - \alpha = 0. \quad (13)$$

There are two regimes of the breathing motion of the skyrmion, if one looks at the behavior of γ. The oscillating regime corresponds to closed trajectories around the metastable energy minimum. The rotating regime is described by γ steadily increasing with time. However, one can reduce γ to the interval $(-\pi, \pi)$. In this representation, in the rotating regime trajectories are leaving the area through the top and reentering through the bottom. The skyrmion size λ is oscillating in both regimes.

Solution of Eq. (13) together with the equation $\partial^2\bar{E}/\partial\bar{\lambda}^2 = 2lh - 1/\bar{\lambda}^4 = 0$ gives the critical field h_c and the value of $\bar{\lambda}_1 = \bar{\lambda}_c =$ at the critical field:

$$h_c = \frac{1}{2l}\left(\frac{3\alpha}{4}\right)^{4/3}, \qquad \bar{\lambda}_c = \left(\frac{4}{3\alpha}\right)^{1/3}. \tag{14}$$

At $h \ll h_c$ one has $\bar{\lambda}_1 \approx \alpha/(2lh)$. This roughly agrees with the lattice results shown in Fig. 4.

To study the dynamics of the spin system, consider the Lagrangian [18,31]

$$\mathcal{L} = \hbar S \int dx\, dy\, \dot{\Phi}(\cos\Theta + 1) - \mathcal{H}, \tag{15}$$

where Θ and Φ are spherical coordinates of $\mathbf{S}$, satisfying $\cos\Theta + 1 = s_z + 1$ and $\tan\Phi = s_y/s_x$. Substituting here Eq. (3), which results in $\dot{\Phi} \equiv d\Phi/dt = \dot{\gamma}$, upon integration one obtains

$$\mathcal{L} = 4\pi\hbar S\dot{\gamma}\bar{\lambda}^2 l - E(\bar{\lambda}, \gamma). \tag{16}$$

The Euler-Lagrange equations are

$$\frac{\partial\mathcal{L}}{\partial\bar{\lambda}} = 0, \quad \frac{d}{dt}\frac{\partial\mathcal{L}}{\partial\dot{\gamma}} = \frac{\partial\mathcal{L}}{\partial\gamma}, \tag{17}$$

resulting in the coupled equations of motion for $\bar{\lambda}$ and γ:

$$2\frac{d\gamma}{dt}\bar{\lambda}l = -\alpha\,\sin\gamma + 2h\bar{\lambda}l + \frac{1}{3\bar{\lambda}^3}, \tag{18}$$

$$2\frac{d\lambda}{dt}l = \alpha\,\cos\gamma. \tag{19}$$

Linearization of the above equations for small-amplitude oscillations yields the frequency of the breathing mode,

$$\bar{\omega}_1(h) = \frac{\hbar\omega}{JS} = \frac{\alpha^{1/2}}{2l\bar{\lambda}_1^{1/2}}\sqrt{2lh - \frac{1}{\bar{\lambda}_1^4}}, \tag{20}$$

where $\bar{\lambda}_1(h)$ is given by Eq. (13). Its dependence on the magnetic field for $l = 0.8$ is shown in Fig. 4.

It is easy to see that at $h \ll h_c$ the above equation gives $\bar{\omega}_1 = h[1 - (\bar{\lambda}_c/\bar{\lambda}_1)^3/4] \approx h$. This coincides with the FMR frequency and differs from a more accurate numerical lattice result $\bar{\omega}_1 \approx 0.8h$ that brings the frequency of the breathing mode below the bottom of the spin-wave spectrum in the bulk. The latter does not allow the breathing mode to decay into spin waves and is responsible for its nondissipative dynamics if damping from other sources is not introduced by hand into the equations of motion.

The above method relies on a fitting parameter l to come close to the numerically obtained critical field. Although this simple method provides a physical picture of the breathing-mode dynamics and provides qualitatively correct results including the maximum of the breathing-mode frequency, there are discrepancies with the numerical solution both near the skyrmion collapse and at low fields. At small fields, the skyrmion becomes large and departs significantly from the shape we use. This must be the reason why our method does not capture the slope at weak fields.

B. Semianalytical approach using corrected skyrmion shape

A better approximation not using any fitting parameters can be developed if one takes into account the deformation of the BP shape of the skyrmion at large distances. Because of the applied field H, the spin field approaches its background value -1 exponentially at the magnetic length $\delta_H = a\sqrt{JS/|H|}$. In the limit $\lambda \ll \delta_H$, the asymptotic solution of the linearized equation for $\mathbf{s}(\mathbf{r})$ at $r \gg \lambda$ can be combined with the BP solution at $r \ll \delta_H$. This leads to replacement of Eq. (3) by

$$\begin{Bmatrix} s_x \\ s_y \end{Bmatrix} = \frac{2\lambda f(r)}{f^2(r) + \lambda^2}\begin{Bmatrix} \cos(\phi + \gamma) \\ \sin(\phi + \gamma) \end{Bmatrix}, \quad s_z = \frac{\lambda^2 - f^2(r)}{\lambda^2 + f^2(r)}, \tag{21}$$

where $f(r) = \delta_H/K_1(r/\delta_H)$ and K_1 is the MacDonald function (see, e.g, Ref. [21]). Although formally valid for $\lambda \ll \delta_H$, this solution that rescales the distance from the skyrmion's center proves to be remarkably robust and provides good results in a wide range of H. The reason is that the actual skyrmion profile obtained numerically or within this approximation always satisfies $\lambda \lesssim \delta_H$, whereas the opposite limit is never realized.

Substitution of Eq. (21) into Eq. (15) gives

$$\mathcal{L} = \hbar\dot{\gamma}\mathcal{M}(\lambda) - E(\lambda, \gamma), \tag{22}$$

where

$$\mathcal{M}(\lambda) = \int dx\, dy \frac{2\lambda^2}{f^2(r) + \lambda^2} \tag{23}$$

is the magnetic moment of the skyrmion and $E(\lambda, \gamma)$ is the energy (11) corresponding to the modified profile of the skyrmion.

The coupled equations of motion for $\mathcal{M}$ and γ that follow from Eq. (17) are

$$\hbar\frac{d\gamma}{dt}\frac{d\mathcal{M}}{d\lambda} = \frac{dE}{d\lambda}, \quad \hbar\frac{d\lambda}{dt}\frac{d\mathcal{M}}{d\lambda} = -\frac{dE}{d\gamma}. \tag{24}$$

For small oscillations $\delta\lambda$ and $\delta\gamma$, near their equilibrium values $\delta\lambda_1$ and $\delta\gamma_1$, approximating the energy by a parabola,

$$E(\lambda, \gamma) = E(\lambda_1, \gamma_1) + \tfrac{1}{2}E_{\lambda\lambda}\delta\lambda^2 + \tfrac{1}{2}E_{\gamma\gamma}\delta\gamma^2, \tag{25}$$

one obtains linear equations of motion

$$\frac{d\delta\gamma}{dt} = \frac{E_{\lambda\lambda}}{\hbar\mathcal{M}_\lambda}\delta\lambda, \quad \frac{d\delta\lambda}{dt} = -\frac{E_{\gamma\gamma}}{\hbar\mathcal{M}_\lambda}\delta\gamma, \tag{26}$$

where $E_{\lambda\lambda} \equiv \partial^2 E/\partial\lambda^2$, $E_{\gamma\gamma} \equiv \partial^2 E/\partial\gamma^2$, and $\mathcal{M}_\lambda \equiv d\mathcal{M}/d\lambda$. These equations describe the oscillating motion of the dynamically conjugate pair $\{\delta\lambda, \delta\gamma\}$ at a frequency

$$\omega = \sqrt{\frac{E_{\lambda\lambda}E_{\gamma\gamma}}{\hbar\mathcal{M}_\lambda}}. \tag{27}$$

This solution is more general than the one given above and it reproduces Eq. (20) if the BP skyrmion profile is used.

The energy $E(\lambda, \gamma)$ should now be computed numerically with the help of Eqs. (11) and (21) and minimized with respect to λ and γ to obtain their equilibrium values. This gives $\gamma = \pi/2$ as before. The corresponding shape and equilibrium size of the skyrmion computed that way and compared with

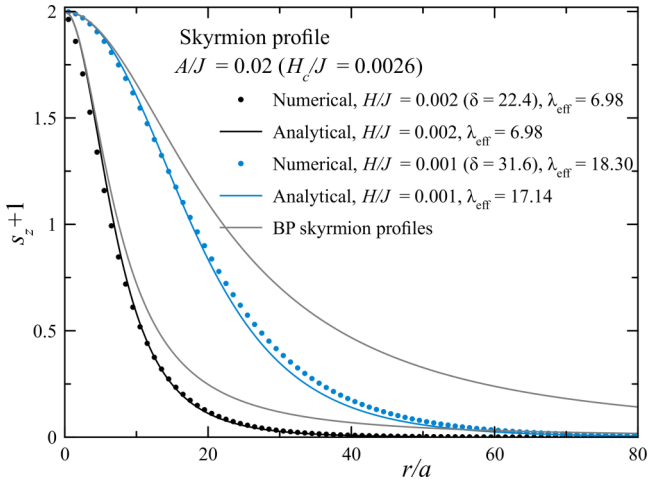

FIG. 10. Modified skyrmion shape given by Eq. (21) with the equilibrium size $\lambda_{\rm eff}$ obtained by the numerical minimization of the energy for two values of the magnetic field $H/J = 0.001$ and $H/J = 0.002$ below the critical field $H_c/J = 0.0026$. Comparison with the BP shape and numerical results obtained on the lattice are also shown.

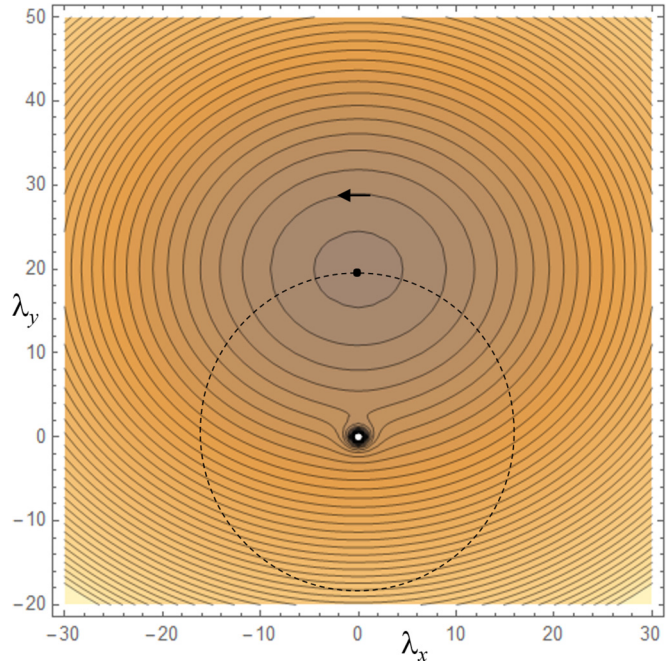

FIG. 11. Equipotential lines in the $\{\lambda_x, \lambda_y\} = \{\lambda\cos\gamma, \lambda\sin\gamma\}$ plane corresponding to Eq. (12) with $l = \text{const}$. Dashed circle corresponds to changing the chirality angle γ of the equilibrium skyrmion.

numerical results on the lattice are illustrated in Fig. 10. Deviation from the BP shape at large distances from the center of the skyrmion is quite significant while disagreement between our semi-analytical model and numerical results obtained on the lattice is rather small.

A better agreement with numerical results on the lattice (achieved in the absence of any fitting parameter) can also be seen in the plot of $\omega(H)$ of Eq. (27) shown by red line in Fig. 4. In particular, the semianalytical approach provides a much better description of the collapse region than the crude analytical approach. However, the correct slope 0.8 in the low field $\omega(H)$ is not captured.

IV. LARGE-AMPLITUDE BREATHING MODE

In this section, we investigate numerically the dynamics of large-amplitude breathing mode initiated by rotating the spins by a large angle $\Delta\gamma$. Instead of the phase diagram in terms of $\{\lambda, \gamma\}$ shown in Fig. 9, it is more convenient to use the phase diagram in terms of $\{\lambda_x, \lambda_y\} = \{\lambda\cos\gamma, \lambda\sin\gamma\}$. For the same parameters as Fig. 9, this new phase diagram is shown in Fig. 11. Here, all equipotential lines are closed. Oscillating regime corresponds to equipotential lines that do not enclose the center $\{0, 0\}$ where the skyrmion collapses. Rotating regime corresponds to the lines that do enclose the center, $\lambda = 0$. Rotation of the spins by the angle $\Delta\gamma$ out of the equilibrium point denoted by the dot, corresponds to the displacement along the dashed circle around the center. The findings of our lattice model complement the results of Ref. [32] that considered the same problem within a modified Lagrangian approach.

Numerical results in Fig. 12 (upper panel) for the model of 500×500 spins without PMA with $A/J = 0.02$ and $H/J = -0.001$ show that stable breathing motion is possible for $\Delta\gamma < 45^\circ$, although this motion is clearly affected by the coupling to other modes. For larger amplitudes, the skyrmion collapses approaching the collapse point either directly ($\Delta\gamma = 50^\circ$ and 60°) or after one rotation ($\Delta\gamma = 90^\circ$, 120°, and 180°). Such a quick dissipation of the energy of the breathing mode is due to the energy transfer into the other modes, whereas the total energy of the system is conserved. As the measured frequency of the large-amplitude breathing modes ($\omega = 0.000\,929$, $0.000\,988$, and $0.001\,064\,9$ in units of $J/\hbar$ for $\Delta\gamma = 90^\circ$, 120°, and 170°, respectively), approaches the FMR frequency, Eq. (10), that yields $\omega_{\rm FMR} = 0.001$, the energy transfer into the FMR mode becomes possible. This is not surprising because the rotational breathing mode evolves in the same direction, thus it can efficiently drive the bulk precession mode, losing its energy. To the contrary, motion of γ back and forth in the oscillating regime cannot drive the bulk precession mode. When the skyrmion collapses, its entire energy is converted into that of spin waves.

Numerical results in the lower panel of Fig. 12 computed for the same model with the PMA added, $D/J = 0.002$, show a smaller basin of small-amplitude breathing mode. There is a periodic motion around the energy minimum for the deviation angle $\Delta\gamma = 10^\circ$ but already for $\Delta\gamma = 20^\circ$ the skyrmion collapses. This can be explained by the smaller equilibrium skyrmion size ($\lambda/a = 6.13$ compared to $\lambda/a = 18.3$ for the model with no PMA) and thus its closeness to the collapse.

Comparing to the model without PMA, the large-amplitude breathing mode with the initial spin rotation $\Delta\gamma = 180^\circ$ is more resilient and ends in the collapse only after four oscillations (see Fig. 13). This can be explained by the frequency mismatch between this mode ($\omega = 0.0024$) and the bulk precession mode for which Eq. (10) yields $\omega_{\rm FMR} = 0.003$. This mismatch makes the process of the energy transfer from the large-amplitude breathing mode to spin waves nonresonant.

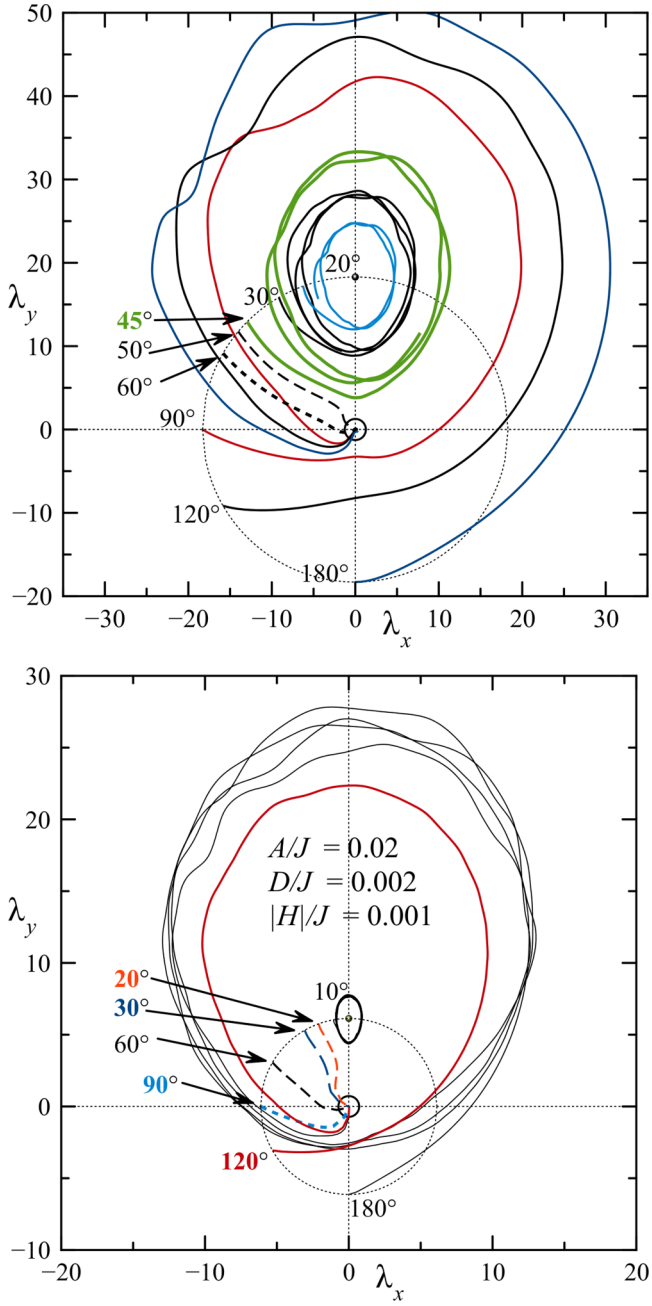

FIG. 12. Dynamics of the breathing mode after rotating of the spins by the angle $\Delta\gamma$ in the system of 500×500 spins with $A/J = 0.02$ and $H/J = -0.001$. Upper panel: no PMA; for $\Delta\gamma \gtrsim 50^\circ$, the skyrmion collapses fast. Lower panel: $D/J = 0.002$; for $\Delta\gamma \gtrsim 10^\circ$, the skyrmion collapses.

Finally, we investigated the dynamics of the breathing mode in zero field for the same parameters $A/J = 0.02$, $D/J = 0.002$ on the 500×500 lattice. Here, the equilibrium skyrmion size is $\lambda = 23.15$ (see Fig. 2). In this case, the breathing mode is very slow with the frequency far below the spin-wave band $\omega_{\rm FMR} = 0.002$. This precludes transfer of the energy of the breathing mode into that of spin waves and makes the breathing mode undamped within our approach. The trajectories shown in Fig. 14 are closed (apart from small fluctuations) for most of the values of $\Delta\gamma$, except the region

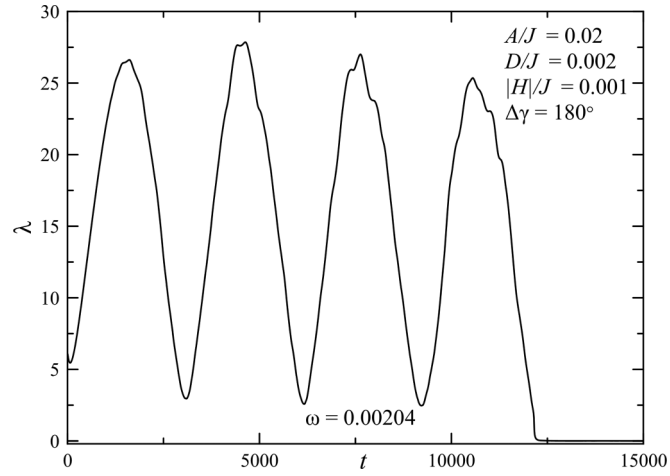

FIG. 13. Time dependence of the skyrmion size λ in the model with $A/J = 0.02$, $D/J = 0.002$, and $H/J = -0.001$ after the initial rotation of spins $\Delta\gamma = 180^\circ$. After four oscillations, the skyrmion collapses.

$40^\circ \lesssim \Delta\gamma \lesssim 70^\circ$ in which the skyrmion's trajectory directly approaches the collapse point. (Note that within the effective theory of Sec. III the skyrmion cannot collapse because of the energy conservation.) The frequency of the breathing mode is $\omega = 0.000\,670$ for $\Delta\gamma = 10^\circ$ and $\omega = 0.000\,338$ for $\Delta\gamma = 180^\circ$. These are almost by an order of magnitude lower than $\omega_{\rm FMR}$ that explains the absence of the intrinsic damping.

Time dependence $\lambda(t)$ for $\Delta\gamma = 180^\circ$ is shown in Fig. 15. The motion is nearly perfectly periodic, except of small irregularities. It is visibly anharmonic with λ changing slower when it is large and faster when it is small.

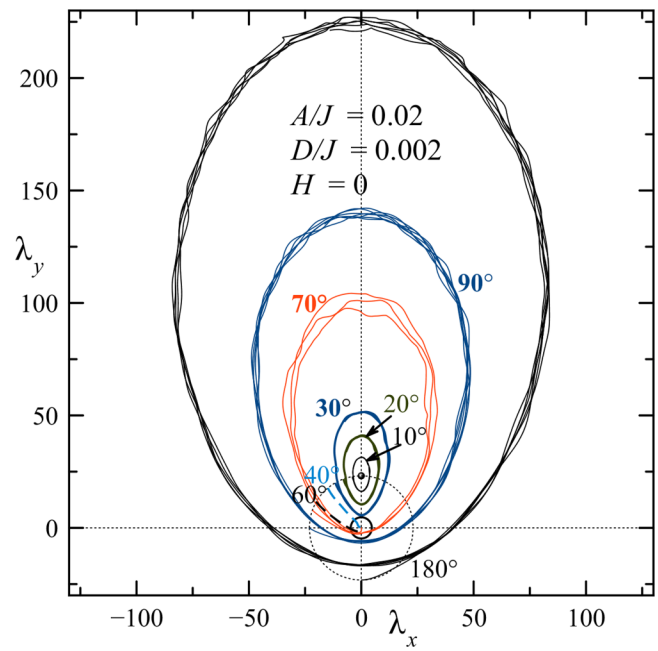

FIG. 14. Dynamics of the breathing mode after rotation of the spins by the angle $\Delta\gamma$ in the system of 500×500 spins with $A/J = 0.02$, $D/J = 0.002$, and $H = 0$. Here, breathing mode collapses only in the range $40^\circ \lesssim \Delta\gamma \lesssim 70^\circ$.

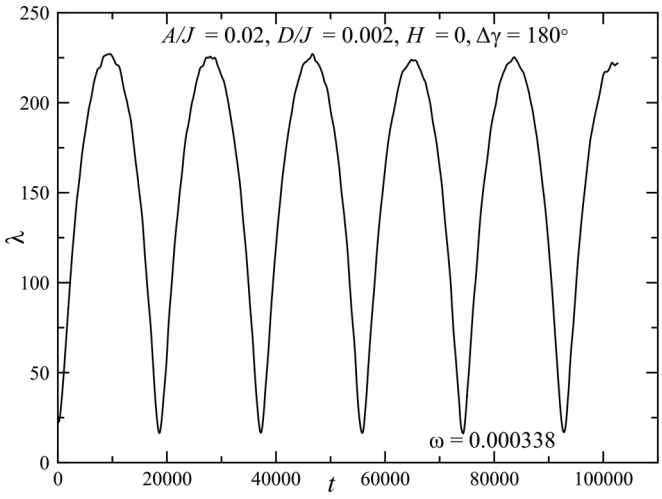

FIG. 15. Time dependence of the skyrmion size λ in the model with $A/J = 0.02$, $D/J = 0.002$, and $H = 0$ after the initial rotation of spins $\Delta\gamma = 180^\circ$. This large-amplitude breathing mode is very slow and undamped.

If a small phenomenological damping is added via the Landau-Lifshitz equation, trajectories of the small-amplitude breathing modes will spiral down to the energy minimum corresponding to the equilibrium skyrmion. Trajectories of large-amplitude breathing modes will spiral down and eventually hit the collapse point $\lambda = 0$.

V. CONCLUSIONS

We have studied the breathing mode of a skyrmion stabilized by the Dzyaloshinskii-Moriya interaction in a noncentrosymmetric magnetic film. In agreement with other authors [26–28] we show that the frequency of the small-amplitude breathing mode is linear on the field in a broad field range with the slope close to 80% of the FMR slope. It reaches maximum on increasing the field, and then tends to zero on approaching the critical field above which the skyrmion collapses. Remarkably, that 0.8 slope appears to be a universal number independent of the strength of the DMI.

The above behavior of the breathing mode has been obtained by us using three methods: Computations on lattices up to 500×500 in size; crude analytical approximation using the Belavin-Polyakov shape of the skyrmion; and a semianalytical dynamical model based upon modified skyrmion shape. All three models have produced qualitatively similar behavior. They agree with each other quantitatively within 20%. Our analytical approach provides a simple physical picture of the breathing mode as coupled oscillations of the skyrmion size and magnetic moment.

The numerical model on the lattice, which is the most accurate of the three, confirms that the frequency of the breathing mode in the oscillating low-amplitude regime is always below the excitation spectrum in the bulk. This, together with the spin precession back and forth, precludes the decay into spin waves in which spin precession goes in one direction. This explains why no damping of the low-amplitude breathing oscillation of the skyrmion has been observed in the numerical experiment within the conservative spin model. In real experiments the damping may result from coupling to phonons and conducting electrons. Such damping, which is expected to be weak in insulating materials, must lead to a slow exponential decay of the low-amplitude breathing mode as suggested in Ref. [32].

For large-amplitude oscillations of the skyrmion, the chirality angle increases monotonically instead of oscillating. Due to nonlinearities, the frequency of such oscillations increases with increasing amplitude and eventually comes into resonance with the bulk precession mode. The spins in that breathing mode rotate in the same direction, allowing direct transformation of its energy into spin waves. At sufficiently small amplitude, such a breathing mode is stable but above a certain threshold it becomes strongly damped. In such a dissipative process the size of the skyrmion decreases, leading to its eventual collapse with the energy of the skyrmion converted into the energy of spin waves. This result complements the findings of Ref. [32] regarding dissipative dynamics of the rotational mode.

Adding perpendicular anisotropy and removing the applied field makes the breathing mode very slow and far below the spin-wave band. As the result, the processes of intrinsic relaxation are prohibited and the breathing mode is undamped in the absence of phenomenological damping.

Current-induced spin torques have been used to manipulate skyrmions [7]. In such experiments, the breathing dynamics could be used to control skyrmion transport through a constriction [6]. If skyrmions are utilized for data storage and processing, our theory developed for the smallest skyrmions must be useful for analyzing their response to external perturbations.

ACKNOWLEDGMENTS

This work has been supported by the Grant No. DE-FG02-93ER45487 funded by the US Department of Energy, Office of Science.

[1] N. Nagaosa and Y. Tokura, Nat. Nanotechnol. **8**, 899 (2013).
[2] R. Tomasello, E. Martinez, R. Zivieri, L. Torres, M. Carpentieri, and G. Finocchio, Nat. Sci. Rep. **4**, 6784 (2014).
[3] X. Zhang, M. Ezawa, and Y. Zhou, Sci. Rep. **5**, 9400 (2015).
[4] G. Finocchio, F. Büttner, R. Tomasello, M. Carpentieri, and M. Klaui, J. Phys. D: Appl. Phys. **49**, 423001 (2016).
[5] A. O. Leonov, T. L. Monchesky, N. Romming, A. Kubetzka, A. N. Bogdanov, and R. Wiesendanger, New J. Phys. **18**, 065003 (2016).
[6] W. Jiang, G. Chen, K. Liu, J. Zang, S. G. E. te Velthuis, and A. Hoffmann, Phys. Rep. **704**, 1 (2017).
[7] A. Fert, N. Reyren, and V. Cros, Nat. Rev. Mater. **2**, 17031 (2017).

[8] T. H. R. Skyrme, Proc. R. Soc. A **247**, 260 (1958).
[9] N. Manton and P. Sutcliffe, *Topological Solitons* (Cambridge University Press, Cambridge, 2004).
[10] A. A. Belavin and A. M. Polyakov, Pis'ma Zh. Eksp. Teor. Fiz **22**, 503 (1975) [Sov. Phys.–JETP Lett. **22**, 245 (1975)].
[11] E. M. Chudnovsky and J. Tejada, *Lectures on Magnetism* (Rinton, Princeton, NJ, 2006).
[12] L. Cai, E. M. Chudnovsky, and D. A. Garanin, Phys. Rev. B **86**, 024429 (2012).
[13] F. Buttner, I. Lemesh, and G. S. D. Beach, Sci. Rep. **8**, 4464 (2018).
[14] O. Boulle, J. Vogel, H. Yang, S. Pizzini, D. S. de Souza Chaves, A. Locatelli, T. O. Mentes, A. Sala, L. D. Buda-Prejbeanu, O. Klein, M. Belmeguenai, Y. Roussigné, Y. A. Stashkevich, S. M. Chérif, L. Aballe, M. Foerster, M. Chshiev, S. Auffret, I. M. Miron, and G. Gaudin, Nat. Nanotechnol. **11**, 449 (2016).
[15] C. Moreau-Luchaire, C. Moutas, N. Reyren, J. Sampaio, C. A. F. Vaz, N. Van Horne, K. Bouzehouane, C. Gar-cia, K. Deranlot, P. Warnicke, P. Wohlhter, J.-M. George, M. Weigand, J. Raabe, V. Cros, and A. Fert, Nat. Nanotechnol. **11**, 444 (2016).
[16] N. Romming, C. Hanneken, M. Menzel, J. E. Bickel, B. Wolter, K. von Bergmann, A. Kubetzka, and R. Wiesendanger, Science **341**, 636 (2013).
[17] N. Romming, A. Kubetzka, C. Hanneken, K. von Bergmann, and R. Wiesendanger, Phys. Rev. Lett. **114**, 177203 (2015).
[18] A. Derras-Chouk, E. M. Chudnovsky, and D. A. Garanin, Phys. Rev. B **98**, 024423 (2018).
[19] T. H. O'Dell, *Ferromagnetodynamics: The Dynamics of Magnetic Bubbles, Domains, and Domain Walls* (Wiley, New York, 1981).
[20] E. B. Kaufluss and U.-G. Meissner, Phys. Lett. **154B**, 193 (1985).
[21] V. P. Voronov, B. A. Ivanov, and A. M. Kosevich, Zh. Eksp. Teor. Fiz. **84**, 2235 (1983) [Sov. Phys.–JETP **57**, 1303 (1983)].
[22] See for review: M. Garst, J. Waizner, and D. Grundler, J. Phys. D: Appl. Phys. **50**, 293002 (2017).
[23] M. Mochizuki, Phys. Rev. Lett. **108**, 017601 (2012).
[24] I. Makhfudz, B. Kruger, and O. Tchernyshyov, Phys. Rev. Lett. **109**, 217201 (2012).
[25] Y. Onose, Y. Okamura, S. Seki, S. Ishiwata, and Y. Tokura, Phys. Rev. Lett. **109**, 037603 (2012).
[26] S.-Z. Lin, C. D. Batista, and A. Saxena, Phys. Rev. B **89**, 024415 (2014).
[27] C. Schütte and M. Garst, Phys. Rev. B **90**, 094423 (2014).
[28] L. Rózsa, J. Hagemeister, E. Y. Vedmedenko, and R. Wiesendanger, Phys. Rev. B **98**, 224426 (2018).
[29] J-V. Kim, F. Garcia-Sanchez, J. Sampaio, C. Moreau-Luchaire, V. Cros, and A. Fert, Phys. Rev. B **90**, 064410 (2014).
[30] S.-Z. Lin, Phys. Rev. B **96**, 014407 (2017).
[31] V. P. Kravchuk, D. D. Sheka, U. K. Roßler, J. van den Brink, and Y. Gaididei, Phys. Rev. B **97**, 064403 (2018).
[32] B. F. McKeever, D. R. Rodrigues, D. Pinna, A. Abanov, J. Sinova, and K. Everschor-Sitte, Phys. Rev. B **99**, 054430 (2019).
[33] D. A. Garanin, E. M. Chudnovsky, and T. Proctor, Phys. Rev. B **88**, 224418 (2013).
[34] D. A. Garanin and H. Kachkachi, Phys. Rev. B **80**, 014420 (2009).
[35] L. Desplat, D. Suess, J.-V. Kim, and R. L. Stamps, Phys. Rev. B **98**, 134407 (2018).